Cell sorting is analogous to phase ordering in fluids

D. A. Beysens*, G. Forgacs[†‡], and J. A. Glazier[§¶]

*ESEME–Service des Basses Temperatures, Commissariat à l'Energie Atomique, 38054 Grenoble, France; [†]Department of Physics and Biology, Clarkson University, Potsdam, NY 13699-5820; [‡]Department of Physics and Biology, University of Missouri, Columbia, MO 65211; and [§]Department of Physics, 316 Nieuwland, University of Notre Dame, Notre Dame, IN 46556

Edited by Joel L. Lebowitz, Rutgers The State University of New Jersey–New Brunswick, Piscataway, NJ, and approved June 2, 2000 (received for review February 10, 2000)

Morphogenetic processes, like sorting or spreading of tissues, characterize early embryonic development. An analogy between viscoelastic fluids and certain properties of embryonic tissues helps interpret these phenomena. The values of tissue-specific surface tensions are consistent with the equilibrium configurations that the Differential Adhesion Hypothesis predicts such tissues reach after sorting and spreading. Here we extend the fluid analogy to cellular kinetics. The same formalism applies to recent experiments on the kinetics of phase ordering in two-phase fluids. Our results provide biologically relevant information on the strength of binding between cell adhesion molecules under near-physiological conditions.

Knowing the molecular binding strength between cell adhesion molecules is crucial to understanding morphogenesis. Atomic force microscopy can measure the strength of bonds between individual biological receptor molecules and their ligands (1–4). Because the properties of these molecules strongly depend on their extracellular and intracellular environments, interpreting measurements of the binding energy outside of tissues biologically may be difficult. However, the analogy between cell sorting and the separation of immiscible fluids provides important quantitative information on the effective binding energy between cell adhesion molecules *in situ* under near-physiological conditions.

Certain embryonic tissues mimic the behavior of viscous liquids or fluids (5). Often during embryonic morphogenesis one cell population spreads over the surface of another, in the manner of a liquid spreading on a solid or on another liquid. In suspension or on nonadhesive surfaces, various multicellular aggregates round just as liquid droplets do. Cells of two distinct tissues randomly intermixed within such aggregates sort out into separate regions like coalescing droplets of immiscible liquids. Such behavior requires (*i*) many subunits, which (*ii*) cohere while (*iii*) being mobile. In ordinary liquids, the subunits are molecules or droplets; in rearranging cell populations, the subunits are living cells. The interaction potential between both liquid and cellular subunits is of a Lenard–Jones type: hard sphere repulsion and short and longer range attraction. In liquids, van der Waals forces mainly cause the attraction while cells interact via cell adhesion molecules at short distances and via steric interactions caused by long filopodia at a range of a few cell diameters. Filopodia may be significant at low cell density but are absent in the close-packed tissues we study. In liquids, the mobility of the subunits is thermal; in tissues, it is "amoeboid." Despite these differences, shared properties cause tissues whose cells are mobile to behave in many respects like fluids.

To account for the fluid-like behavior of cell populations, Steinberg formulated the "differential adhesion hypothesis," or DAH (6, 7), according to which differential expression of adhesion molecules guides certain morphogenetic movements. Recent experimental results support the DAH (8, 9). Furthermore, the DAH implies that, as in liquids, adhesive and cohesive interactions between the component subunits generate surface and interfacial tensions, which cause the observed behavior of embryonic cell populations. Surface adhesion molecules cause cells to "stick" strongly to each other. Thus on a deeper level a tissue is analogous to an "associative fluid" (10, 11) rather than to a weakly interactive liquid. Recent experiments have demonstrated that, (*i*) tissue surface tension is a well-defined intensive physical parameter that characterizes the equilibrium shape of certain multicellular aggregates (12), and (*ii*) the measured values of these tensions account for the observed mutual envelopment and sorting behavior of the corresponding tissues (13). Computer simulations applying the principles of the DAH by using specific statistical mechanical models reproduce the equilibrium configurations seen in cell-sorting experiments (14, 15).

Surface tension is an equilibrium property. Even if differences in surface tension drive movement during morphogenesis, by themselves they reveal little about the movement's time course. The kinetics of cell sorting and tissue envelopment depends on the dynamical properties of cell populations. Early experiments by Phillips *et al.* (16, 17) showed that embryonic cell aggregates behave like deformable solids during brief experimental manipulations and like viscous liquids in long-term organ cultures. We expect tissues to be complex viscoelastic materials because the major components of cells are viscoelastic. The viscoelastic moduli of the cytoplasm of various cells have been measured (18–24). Detailed experiments on the viscoelasticity of solutions of major cytoplasmic biopolymers like microtubules, actin microfilaments, and intermediate filaments suggest possible specialized roles for the different classes of filaments *in vivo* (25–28). From the deformations of red blood cells, Engelhardt and Sackmann (29) determined the shear elastic moduli and viscosities of erythrocyte plasma membranes. Davidson *et al.* studied the viscoelastic response of the cellular and extracellular layer in mesenchyme blastula stage sea urchin embryos (30) to distinguish between various models of primary invagination preceding gastrulation. Finally, Forgacs *et al.* recently measured the viscoelastic moduli of embryonic cell aggregates (i.e., model tissues) (31).

In this work, we analyze cell sorting and single-cell motion in a cluster of dissimilar cells in terms of concepts of fluid mechanics. We demonstrate that the fluid model of tissues explains both the equilibrium configuration reached in sorting and the time evolution (i.e., kinetics) and morphology of the developing cellular pattern. This analogy allows us to estimate the binding energy of typical cell adhesion molecules under near physiological conditions.

Materials, Methods, and Concepts

Sample Preparation. We dissected eyes from 4-day fertile white leghorn chicken eggs (Avian Services, Frenchtown, NJ) and incubated in PBS + 2.5% porcine trypsin (GIBCO/BRL catalogue no. 15090–046) + 1% pancreatin (GIBCO/BRL) for 15

This paper was submitted directly (Track II) to the PNAS office.

Abbreviations: T_{cx}, coexistence temperature; T_c, critical temperature.

[¶]To whom reprint requests should be addressed. E-mail: forgacs@clarkson.edu.

The publication costs of this article were defrayed in part by page charge payment. This article must therefore be hereby marked "*advertisement*" in accordance with 18 U.S.C. §1734 solely to indicate this fact.

min. We separated the thin pigmented layer from the neural layer with forceps. To break up the extracellular matrix, we incubated the neural and pigmented tissues in trypsin-EDTA (GIBCO/BRL catalogue no. 15400–096) for 25 and 50 min, respectively, and washed them three times in PBS. We mechanically dispersed the dissociated tissues by gentle pipetting in DMEM with Earle's salts, containing 10% horse serum (HyClone), 50 μg/ml DNase I (Boehringer Mannheim), 70 μg/ml gentamycin, 50 μg/ml penicillin-streptomycin-neomycin, and 50 μg/ml kanamycin (GIBCO/BRL). We washed dispersed cells in the same solution.

Sorting. We mixed the two cell types in ratios ranging from 3 to 10 neural cells per pigmented cell. We cultured the mixtures in cell medium in a controlled temperature gyratory shaker (Lab-Line Instruments; diameter of gyration 7.5 cm) at 37°C. After 8–12 h, when cells adhered to form compact aggregates, we transferred some aggregates to be cultured singly at 37°C in specially designed observation chambers. We observed aggregates, ranging in diameter from 150 to 300 μm with an inverted optical microscope [Olympus (New Hyde Park, NY) IMT2], capturing images and digitizing them at regular time intervals.

Single-Cell Tracking. Using the sorting protocol with extremely dilute cell mixtures (one pigmented cell for 100 neural retina cells) and tracking the pigmented cells for 30 h at intervals of 30 min, we measured the diffusion constant of these cells as described in ref. 32. Measurement of velocity autocorrelation functions revealed that on this time scale, single-cell motion was indeed diffusive (32).

Measurement of Cell Size. We determined cell size in cell suspensions by using a calibrated stage micrometer and a compound microscope (Olympus BH-2).

Tissue Surface Tension and Viscoelastic Properties. We adjusted supernatants containing suspensions of either separated neural retinal or pigmented epithelial cells to a concentration of 10^6 cells/ml and transferred 3 ml to 10-ml tissue culture flasks (Bellco Glass). We placed the flasks in a water bath/shaker (Lab-Line) at 37°C, 5% CO_2 for 2–4 h at 120 rpm, then transferred 3–4 $\times$ 10^6 cells per tube to round-bottom glass tubes 15 mm in diameter and centrifuged and cultured them until they formed firm thin pellets (usually 2–4 h, depending on tissue type). We then cut these pellets into fragments about 1 mm in diameter and incubated them on a gyratory shaker (Lab-Line; diameter of gyration, 7.5 cm) at 120 rpm under 5% CO_2 at 37°C until the fragments rounded up (1.5–2 days, depending on tissue type).

Fig. 1 shows the parallel plate compression apparatus used to measure the viscoelastic properties of living embryonic tissues. We have described elsewhere details of its operation (12, 13). Briefly, we compressed aggregates of 30,000–40,000 cells, ranging in diameter from 200 μm to about 600 μm, between the parallel plates of the apparatus in sterile Eagle's MEM containing Hanks' balanced salt solution, 10% horse serum, and antibiotics (see above) at 37°C. We positioned the aggregate (A) on the lower compression plate (LCP) in the inner chamber (IC). A circulating water bath (Lauda) maintains the water temperature in the outer chamber (OC) at 37°C. Coating the compression plates with poly(2-hydroxyethylmethacrylate) [poly(HEMA)] (30) minimizes the adherence of the aggregate to the plate. The upper compression plate (UCP) hangs from the arm of a Cahn/Ventron (Cerritos, CA) Model 2000 recording electrobalance (through a nickel-chromium wire, NCW). Recording its apparent weight establishes a precompression zero force baseline. Raising the LCP by turning the lower assembly (LA) compresses the aggregate between the two plates. We monitored

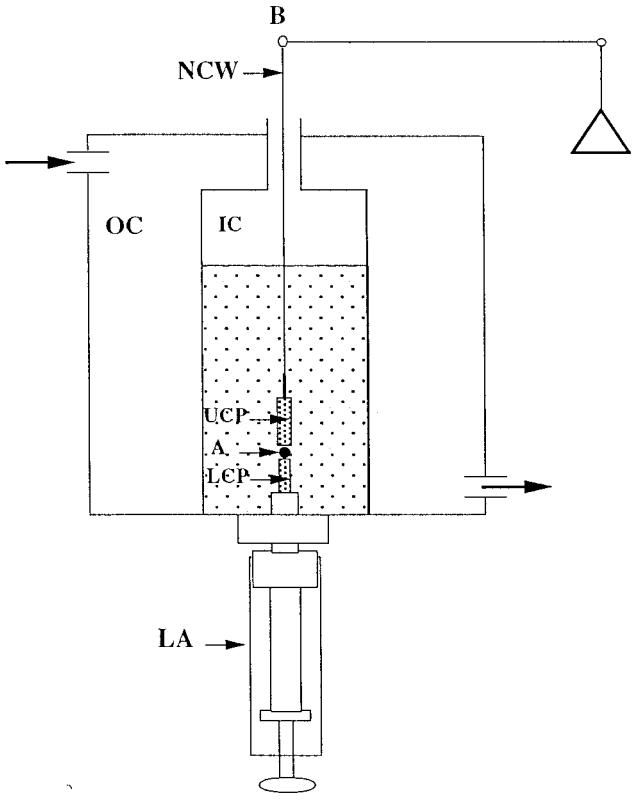

Fig. 1. Schematic representation of the compression plate apparatus used to measure tissue surface tension and viscoelastic properties.

the shape of the aggregate through a horizontally positioned microscope (Olympus SZ60) and recorded it with two video cameras (MTI 72 and Javelin color CCD, placed at a 90° angle relative to each other) by using a Panasonic (Seacaucus, NJ) time-lapse video recorder. A Micron Millenia Pro2 computer equipped with a National Instrument Multifunction I/O (National Instruments, Austin, TX) card and LABVIEW software for data acquisition and a composite color PCI frame grabber (Data Translation, Marlboro, MA) continuously recorded changes in the force exerted by the aggregate on the UCP, equal to the change in the latter's apparent weight.

Fig. 2 shows a typical force relaxation curve. Laplace's equation determines the tissue surface tension (33) from the equilibrium value of the compressive force in Fig. 2, as described in

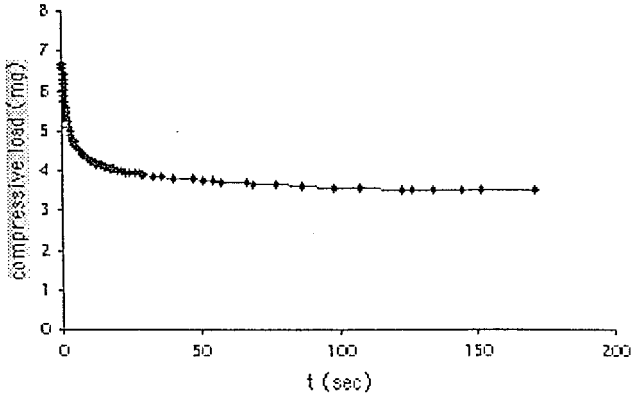

Fig. 2. Typical force relaxation in a chicken heart cell aggregate after compression.

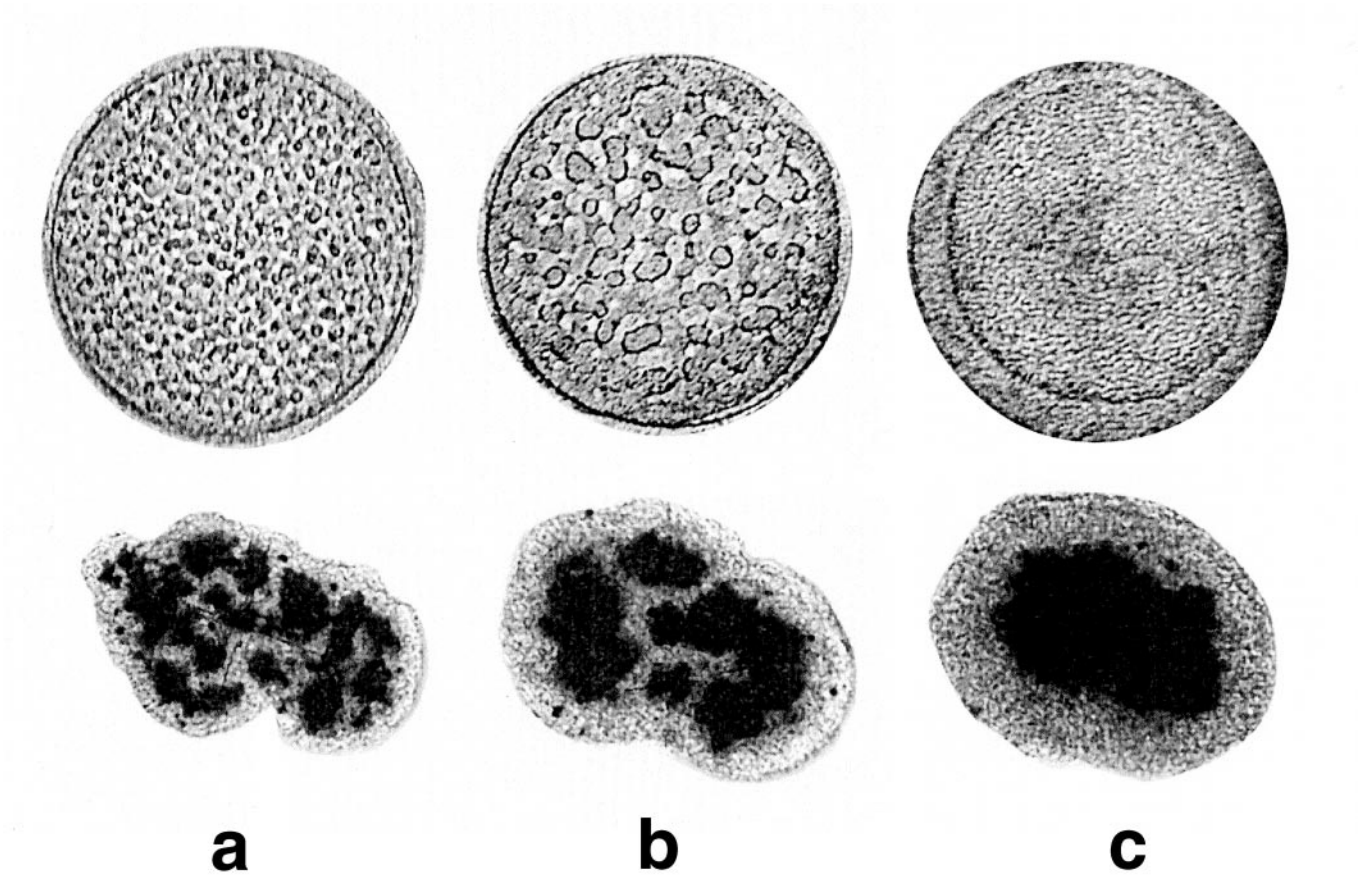

Fig. 3. (*Upper*) Gas and liquid phase ordering in SF_6 under reduced gravity, after a thermal quench of 0.7 mK below the critical point (45.564°C). The container diameter is 12 mm. Gas and liquid eventually order with the liquid phase wetting the container wall and surrounding the gas phase, corresponding to $\sigma_{wl} < \sigma_{wg}$, where σ_{wl} and σ_{wg} are the wall-liquid and the wall-gas interfacial tensions, respectively. *a*, *b*, and *c* correspond to 120 s, 275 s and 3,960 s after quench, respectively. (*Lower*) Sorting out of chicken embryonic pigmented epithelial cells (dark) from chicken embryonic neural retinal cells (light). The average aggregate size is 200 μm. At the end of sorting, neural retinal cells preferentially wet the external tissue culture medium surrounding the aggregates. σ_{tn}(= 1.6 dyne/cm)$<\sigma_{tp}$(= 12.6 dyne/cm)[3], where σ_{tn} and σ_{tp} are the tissue culture medium-neural retina and the tissue culture medium-pigmented epithelium interfacial tensions, respectively. *a*, *b*, and *c* correspond to 17 h, 42 h, and 73 h after initiation of sorting, respectively.

ref. 13. Tissue surface tension refers to interfacial tension between the tissue and the surrounding tissue culture medium, which is always present. We evaluated tissue viscoelastic properties by using a generalized Kelvin model (34) of viscoelasticity, fit to the entire curve in Fig. 2, as given in ref. 31.

Phase Ordering in Fluids Under Microgravity. The experiment took place in the French ALICE facility on the Mir space station during the Cassiopée mission (August 17, 1996–September 2, 1996). A copper-beryllium (CuBe) cell with two windows encloses the fluid, SF_6 (Air Liquide, Paris, France), of better than 99.98% purity. The internal volume is a cylinder (12 mm internal diameter, 1.7 mm thickness), with two natural sapphire windows (12 mm external diameter) epoxied on their cylindrical surface to the CuBe wall. To nucleate the nonwetting vapor phase, we increase the density slightly off critical (by 0.25%) on the liquid side, corresponding to a coexistence temperature T_{cx} shifted from T_c by $T_{cx} - T_c = -0.7$ μK. A high-precision thermostat keeps the cell at an initial temperature T_i ($>T_{cx}$). The thermostat is stable to 5 μK controllable in steps of 100 μK. Temperature quenches, at a mean rate of 200 μK/s, last approximately 5 s. In the quenches we analyzed, the sample temperature began to vary approximately 8 s after T_i changed to the final temperature T_f ($<T_{cx}$). The temperature crosses T_{cx} 4 s later, and we analyzed the experiments 8 s later (i.e., 20 s after we set the temperature to T_f). We measured time from the moment the sample crosses T_{cx}. We illuminated the cell with a parallel white light beam and imaged with a charge-coupled device (CCD) camera. In wide field mode, the CCD camera images a planar section of the full sample (12 mm), with thickness of order 0.1 mm, at 30 μm resolution. In microscopic mode, the resolution is 3 μm, the field is 1.2 mm, and the depth of focus is of order 10 μm. We determined the critical temperature T_c by looking in microscopic mode for the appearance of large-scale fluctuations that correspond to the nucleation of a new phase.

Results

Comparison of Cell Sorting and Nucleation in Fluids. Fig. 3 *Upper* shows pattern evolution in sulfur hexafluoride, SF_6, quenched under microgravity (as explained in the previous section), from the isotropic high-temperature phase (at T_{cx} + 3 mK) to below the critical temperature (T_{cx} − 0.7 mK), where it separates and orders into gas and liquid phases. Because we quench to near a critical point, the interfacial tension between vapor and liquid is small. Thus phase ordering is conveniently slow. Fig. 3 *Lower* illustrates phase separation in a mixture of two cell populations, neural retinal and pigmented epithelial cells from embryonic chicken. Here the neutral buoyancy of the cells in the culture medium eliminates gravity effects. The two patterns are strikingly similar; both evolve by the fusion (or coalescence) of domains.

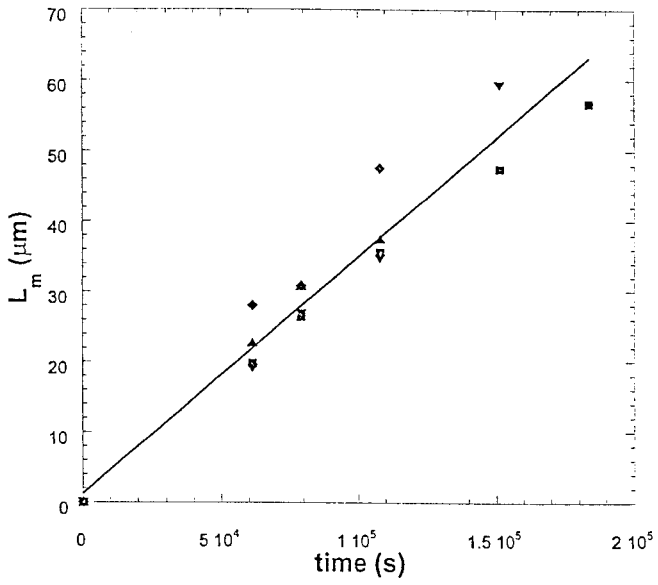

Fig. 4. Time evolution of the pseudoperiod during sorting. Squares, upright and inverted triangles, and diamonds denote four different runs. The fit with a straight line has goodness $R^2 = 0.98$.

In fluids and liquids, interfacial tension between the two phases, σ_1, drives hydrodynamic coalescence, whereas the viscosity, η_1, of the more viscous phase hinders it (35, 36). When the volume fraction of the minority phase exceeds a "critical" value, ϕ ($\approx$0.3), its domains interconnect. The pseudoperiod, L_m, the size of interconnected domains, increases linearly in time, as $L_m = b_l(\sigma_l/\eta_l)t$, with b_l a universal constant, independent of material properties (35). Theory predicts $b_l \approx 0.03$ (37, 38), in agreement with experiments (39).

The cellular aggregate (with $\phi = 0.27$ for the minority pigmented epithelial cells) shown in Fig. 3 has a pseudoperiod that also grows *linearly* in time (see Fig. 4). Measurements with the parallel plate compression apparatus give $\sigma_n = 1.6$ dyne (1 dyne = 10 μN)/cm and $\sigma_p = 12.6$ dyne/cm (13), where σ_n and σ_p are, respectively, the surface tensions of neural retina and pigmented epithelium. At the end of sorting (see Fig. 3), neural retinal cells preferentially wet the interface between pigmented epithelium and the external tissue culture medium. We can thus estimate the neural retina-pigmented epithelium interfacial tension from Young's equation at the onset of complete wetting (32), as $\sigma_t = \sigma_p - \sigma_n \approx 10$ dyne/cm. Complete wetting implies $\sigma_t \leq \sigma_p - \sigma_n$. Viscoelasticity measurements for the viscosity of the (more viscous) pigmented epithelial tissue lead to $\eta_t \approx 10^6$ P (1 P = 0.1 Pa·sec) (31, 40). Finally, the hydrodynamic expression for L_m leads to $b_t \approx 0.003$ (the cellular analogue of b_l), somewhat lower than expected but consistent with the value for fluids given the uncertainties on σ_t and η_t inherent in biological experiments. That tissues and fluids exhibit the same pattern morphology and evolution justifies modeling embryonic cell populations as immiscible fluids, despite a difference of about eight orders of magnitude in the viscosities of fluids and tissues, $\eta_t/\eta_l \approx 10^8$.

Strength of Cellular Binding from Sorting Experiments. In a liquid drop, as in Fig. 3, interfacial capillary fluctuations have thermal origin. If z denotes the displacement perpendicular to an interface, then $\langle z^2 \rangle = (kT/\sigma_l)\ln(D_l/l)$, where $\langle\rangle$ denotes an average over the entire area of the interface, k is Boltzmann's constant, T is absolute temperature, D_l is the linear size of the drop, and l is a minimal characteristic length, identified with the average width of the interface (41, 42).

In the cellular aggregate shown in Fig. 3, fluctuations of the interface separating the two tissues, if present, must have metabolic origin and result from cell membrane ruffling. Sorting requires membrane fluctuations. In the presence of cytochalasin, which suppresses membrane fluctuations and other F-actin mediated processes, sorting is incomplete (43, 44). Computer simulations with reduced fluctuation temperature reproduce sorting patterns in the presence of cytochalasin by (43, 44). Steinberg and Garrod (45, 46) observed ruffling on the surfaces of sorting cells in two-dimensional assays. Rieu *et al.* have measured membrane ruffling at the contacts between autofluorescent *hydra* cells in two-dimensional cell culture (47).

Membrane fluctuations (associated with cytoskeletal rearrangements) break and create adhesive bonds on the surfaces of individual cells. As a consequence, we introduce ε, the cellular analogue of kT, which gives a *measure* (i.e., a lower bound) for the average total effective binding energy per cell. We assume that ε, through cell membrane fluctuations, controls the interfacial fluctuations in our cell mixtures. Cell membrane fluctuations of metabolic origin show a near-thermal spectrum with typical amplitude of order 20% of the diameter of the cell (46) leading to $\langle z^2 \rangle \approx 0.04a^2$, where $a \approx 8$ μm is the linear dimension of a pigmented epithelial cell in the aggregate, and averaging is over the cell area. Using the above relationship between the interface profile and the interfacial tension and replacing kT by ε, we arrive at $\varepsilon = 0.04a^2\sigma_t\ln(D_t/a)$. Here D_t is the linear size of the cell cluster in Fig. 3, $D_t = 200$ μm, so $\varepsilon \approx 8 \times 10^{-8}$ erg (1 erg = 0.1 μJ).

Strength of Cellular Binding from Single-Cell Motion. Mombach and Glazier (32) observed that a single pigmented epithelial cell immersed in an aggregate of neural retinal cells follows a random walk, with a diffusion constant $D \approx 3 \times 10^{-12}$ cm^2/s. If D obeys the Stokes–Einstein relationship relevant for the diffusion of one liquid in another, then $D = kT/[5\pi\eta(a/2)]$. Replacing the thermal energy by the effective fluctuation energy per cell, we obtain $\varepsilon \approx 2 \times 10^{-8}$ erg. The good agreement (within the accuracy of our measurements) between the values of ε obtained by two independent methods suggests that ε controls interfacial fluctuations in cell aggregates.

Discussion

We have analyzed cell movement during sorting in terms of concepts of fluid mechanics. The fluid analogy introduces ε, the fluctuation energy analogous to kT in liquids. Goodwin developed a similar fluctuation or "biological" temperature $W = \varepsilon/k$ to describe the statistical mechanics within cells (48). The numerical result for ε allows us to estimate the effective binding strength between individual pairs of adhesion molecules. In a cellular aggregate like that in Fig. 3, either pigmented epithelial cells, neural retinal cells, or a mixture of the two surround each cell. The adhesion molecules between these cells are not completely identified but are predominantly N- and E-cadherins. The typical number of bound cell adhesion molecules per cell, n, is 10^4–10^5 (49). Using the above result for ε ($\approx 5 \times 10^{-8}$ erg, the average of the two values above) and taking $n = 5 \times 10^4$, we estimate the effective strength of a single cadherin bond *in situ* to be $\approx$10 kcal/mol. Measurement uncertainties allow a range 5–15 kcal/mol.

Cell adhesion molecules typically are complex transmembrane glycoproteins. The attachment of cadherins to the cytoskeleton regulates their homophilic binding (50–54), so the state of the cortical actin network affects the strength of binding between these molecules. Cadherins form adherens junctions, prominent structures in bound cells. Although spe-

cial clustering is not necessary for cadherin function, junctional localization of cadherins probably strengthens intercellular adhesion via lateral association (55). These and other difficulties mask the effective binding strength between cadherins under physiological conditions. Using genetically manipulated E-cadherins under nonphysiological conditions, Koch *et al.* (56) obtained 5.6 kcal/mol for the dissociation energy of a single cadherin dimer.

Our method allows quantitative evaluation of binding strength in a quasiphysiological situation. Prediction requires knowing the adhesion apparatus on the cell surface (which we do not for chicken retinal cells). We could improve our estimates by using genetically transformed cells expressing a single adhesion molecule in controlled quantities. We will use these cells (e.g., murine L-cells transfected with various cadherin genes) in further studies. Because deficiency in cadherin binding correlates with a number of cell malfunctions [e.g., the metastatic potential of certain human tumors (57)], the physical analogy used here could have biomedical significance.

This work was supported by research grants from the National Science Foundation under IBN 97–10010 (G.F.) and INT 96–03035-06 (J.A.G.), by the Petroleum Research Foundation (J.A.G.) and the Centre National d'Etudes Spatiales (D.A.B.). G.F. acknowledges the hospitality of the Collegium Budapest–Institute of Advanced Studies, Hungary, where part of this work was carried out.

1. Lee, G. U., Kidwell, D. A. & Colton, R. J. (1994) *Langmuir* **10,** 354–357.
2. Florin, E. L., Moy, V. T. & Gaub, H. E. (1994) *Science* **264,** 415–417.
3. Moy, V. T., Florin, E. L. & Gaub, H. E. (1994) *Science* **264**, 257–259.
4. Merkel, R., Nassoy, P., Leung, A., Ritchie, K. & Evans, E. (1999) *Nature (London)* **397,** 50–53.
5. Steinberg, M. S. & Poole, T. J. (1982) in *Cell Behavior*, eds. Bellairs, R., Curtis, A. S. G. & Dunn, G. (Cambridge Univ. Press, Cambridge, U.K.), pp. 583–607.
6. Steinberg, M. S. (1963) *Science* **141,** 401–408.
7. Steinberg, M. S. (1998) *Integrative Biology* **1,** 49–59.
8. Godt, D. & Tepass, U. (1998) *Nature (London)* **395,** 387–391.
9. González-Reyes, A. & St. Johnston, D. (1998) *Development (Cambridge, U.K.)* **125,** 2837–2846.
10. Stell, G. & Zhou, Y. (1989) *J. Chem. Phys.* **91,** 3618–3623.
11. Zhou, Y. & Stell, G. (1992) *J. Chem. Phys.* **96,** 1504–1506.
12. Foty, R., Forgacs, G., Pfleger, C. M. & Steinberg, M. S. (1994) *Phys. Rev. Lett.* **14,** 2298–2301.
13. Foty, R., Pfleger, C. M., Forgacs, G. & Steinberg, M. S. (1996) *Development (Cambridge, U.K.)* **122,** 1611–1620.
14. Glazier, J. A. & Graner, F. (1993) *Phys. Rev. E* **47,** 2128–2154.
15. Mombach, J. C. M., Glazier, J. A., Raphael, R. C. & Zajac, M. (1995) *Phys. Rev. Lett.* **75,** 2244–2247.
16. Phillips, H. M. & Steinberg, M. S. (1978) *J. Cell Sci.* **30,** 1–20.
17. Phillips, H. M., Steinberg, M. S. & Lipton, B. H. (1977) *Dev. Biol.* **59,** 124–134.
18. Hiramoto, Y. (1968) *J. Cell Physiol.* **69,** 219–230.
19. Hiramoto, Y. (1969) *Exp. Cell Res.* **56,** 201–208.
20. Valberg, P. A. & Albertini, D. F. (1985) *J. Cell Biol.* **101,** 130–140.
21. Sakanishi, T. Y. (1988) *Biorheology* **25,** 123–128.
22. Hochmuth, R. M., Ting-Beal, H. P., Beaty, B. B., Needham, D. & Tran-Son-Tay, R. (1993) *Biophys. J.* **64,** 1596–1601.
23. Ragsdale, G. K., Phelps, J. & Luby-Phelps, K. (1997) *Biophys. J.* **73,** 2798–2808.
24. Bausch, A. R., Möller, W. & Sackmann, E. (1999) *Biophys. J.* **76,** 573–579.
25. Zaner, K. S. & Valberg, P. A. (1989) *J. Cell. Biol.* **109,** 2233–2243.
26. Müller, O., Gaub, H. E., Bärmann, M. & Sackmann, E. (1991) *Macromolecules* **24,** 3111–3120.
27. Janmey, P. A. (1991) *Curr. Opin. Cell Biol.* **2,** 4–11.
28. Tempel, M., Isenberg, G. & Sackmann, E. (1996) *Phys. Rev. E* **54,** 1802–1810.
29. Engelhardt, H. & Sackmann, E. (1988) *Biophys. J.* **54,** 495–508.
30. Davidson, L. A., Oster, G. F., Keller, R. E. & Koehl, M. A. R. (1999) *Dev. Biol.* **209,** 221–238.
31. Forgacs, G., Foty, R. A., Shafrir, Y. & Steinberg, M. S. (1998) *Biophys. J.* **74,** 2227–2234.
32. Mombach, J. C. M. & Glazier, J. A. (1996) *Phys. Rev. Lett.* **76,** 3032–3035.
33. Rowlinson, J. S. & Widom, B. (1989) *Molecular Theory of Capillarity* (Clarendon, Oxford).
34. Fung, Y. C. (1993) *Biomechanics* (Springer, New York).
35. Siggia, E. (1979) *Phys. Rev. A* **20,** 595–605.
36. Onuki, A. (1994) *Europhys. Lett.* **28,** 175–179.
37. Nikolayev, V. S., Beysens, D. & Guenoun, P. (1996) *Phys. Rev. Lett.* **76,** 3144–3147.
38. San Miguel, M., Grant, M. & Gunton, D. (1985) *Phys. Rev. A* **31,** 1001–1005.
39. Guenoun, P., Gastaud, R., Perrot, F. & Beysens, D. (1987) *Phys. Rev. A* **36,** 4876–4890.
40. Gordon, R., Goel, N. S., Steinberg, M. S. & Wiseman, L. L. (1972) *J. Theor. Biol.* **37,** 43–73.
41. Beysens, D. & Robert, M. (1987) *J. Chem. Phys.* **87,** 3056–3061.
42. Buff, F. P., Lovett, R. A. & Stillinger, F. H. (1965) *Phys. Rev. Lett.* **15,** 621–622.
43. Mombach, J. C. M., Glazier, J. A. Raphael, R. C. & Zajac, M. (1995) *Phys. Rev. Lett.* **75,** 2244–2247.
44. Armstrong, P. B. (1989) *Crit. Rev. Biochem. Mol. Biol.* **24,** 119–149.
45. Garrod, D. R. & Steinberg, M. S. (1973) *Nature (London)* **244,** 568–569.
46. Steinberg, M. S. & Garrod, D. R. (1975) *J. Cell Sci.* **18,** 358–403.
47. Rieu, J. P., Upadhyaya, A., Glazier, J. A., Ouchi, B. & Sawada, Y. (2000) *Biophys. J.*, in press.
48. Goodwin, B. C. (1963) *Temporal Organization in Cells* (Academic, London), pp. 55–79.
49. Lauffenburger, D. A. & Linderman, J. J. (1993) *Receptors* (Oxford Univ. Press, New York).
50. Nagafuchi, A. & Takeichi, M. (1988) *EMBO J.* **7,** 3679–3684.
51. Ozawa, M., Ringwald, M. & Kemler. R. (1990) *Proc. Natl. Acad. Sci. USA* **87,** 4246–4250.
52. Kintner, C. (1992) *Cell* **69,** 225–236.
53. Kemler, R. (1993) *Trends Genet.* **9,** 317–321.
54. Aberle, H., Butz., Stappert, J., Weissig, H., Kemler, R. & Hoschützky, H. (1994) *J. Cell Sci.* **107,** 3655–3663.
55. Gumbiner, B. M. (1996) *Cell* **84,** 345–357.
56. Koch, A. W., Pokutta, S., Lustig, A. & Engel, J. (1997) *Biochemistry* **36,** 7697–7705.
57. Behrens, J., Mareel, M. M., Van Roy, F. M. & Birchmeier, W. (1989) *J. Cell. Biol.* **108,** 2435–2447.